Adaptive optics for ophthalmic applications using a pyramid wavefront sensor

Stéphane R. Chamot and Chris Dainty

Applied Optics, Experimental Physics Department
National University of Ireland Galway, University Road
Galway, Ireland

stephane.chamot@nuigalway.ie

http://optics.nuigalway.ie/index.html

Simone Esposito

Osservatorio Astrofisico di Arcetri, Largo E.Fermi, 5.
50125 Firenze, Italy

esposito@arcetri.astro.it

Abstract: A new adaptive optics system for the eye using a pyramid wavefront sensor interfaced in closed-loop with a piezoelectric deformable mirror is presented. Sensing parameters such as CCD integration time, pupil sampling and beam steering amplitude are tested on the bench and *in vivo* on several volunteers to optimize real-time optical correction. The system allows closed-loop operation at a frame rate of 55 Hz and reduces ocular aberration up to $\lambda/5$ residual RMS over a 6 mm pupil. Aberration correction and mirror control stability clearly increase when smaller beam steering amplitudes synonymous of higher wavefront sensing sensitivity are used. This result suggests that using pyramid wavefront sensors can improve the performance of adaptive-optics system for ophthalmic applications.

OCIS codes: (010.1080) Adaptive optics; (330.4460) Ophthalmic optics; (330.5370) Physiological optics; (330.4300) Noninvasive assessment of the visual system

References and links

1. J. Liang, D. R. Williams, and D. T. Miller, "Supernormal Vision and High-Resolution Retinal Imaging Through Adaptive Optics," J. Opt. Soc. Am. A **14,** 2884–2892 (1997).
2. E. J. Fernandez, I. Iglesias, and P. Artal, "Closed-Loop Adaptive Optics in the Human Eye," Opt. Lett. **26,** 746–748 (2001).
3. A. Roorda, F. Romero-Borja, W. J. I. Donnelly, H. Quenner, T. J. Hebert, and M. C. Campbell, "Adaptive Optics Scanning Laser Ophthalmosopy," Opt. Express **10,** 405–412 (2002), http://www.opticsexpress.org/abstract.cfm?URI=OPEX-10-9-405.
4. M. Glanc, E. Gendron, F. Lacombe, D. Lafaille, J.-F. L. Gargasson, and P. Lena, "Towards Wide-Field Retinal Imaging With Adaptive Optics," Opt. Commun. **230,** 225–228 (2004).
5. B. Hermann, E. J. Fernandez, A. Unterhuber, H. Sattmann, A. F. Fercher, W. Drexler, P. M. Prieto, and P. Artal, "Adaptive-Optics Ultrahigh-Resolution Optical Coherence Tomography," Opt. Lett. **29,** 2142–2144 (2004).
6. Y. Zhang, J. Rha, R. S. Jonnal, D. T. Miller, "Adaptive Optics Parallel Spectral Domain Optical Coherence Tomography for Imaging the Living Retina" Opt. Express **13,** 4792–4811 (2005), http://www.opticsexpress.org/abstract.cfm?URI=OPEX-13-12-4792.
7. B. Platt and R. V. Shack, "Lenticular Hartmann Screen," Opt. Sci. Center Newsl. (University of Arizona) **5,** 15–16 (1971).

#9724 - $15.00 USD Received 28 November 2005; revised 2 January 2006; accepted 5 January 2006

8. R. Ragazzoni, "Pupil Plane Wavefront Sensing With an Oscillating Prism," J. Mod. Opt. **43,** 289–293 (1996).
9. A. Ghedina, M. Cecconi, R. Ragazzoni, J. Farinato, A. Baruffolo, G. Crimi, E. Diolaiti, S. Esposito, L. Fini, M. Ghigo, E. Marchetti, T. Niero, and A. Puglisi, "On Sky Test of the Pyramid Wavefront Sensor," in *Adaptive Optical System II*, P. L.Wizinowich and D. Bonaccini, eds., Proc. SPIE **4839,** 869–877 (2003).
10. R. Ragazzoni and J. Farinato, "Sensitivity of a Pyramidic Wave Front Sensor in Closed Loop Adaptive Optics," Astron. Astrophys. **350,** L23–L26 (1999).
11. S. Esposito and A. Riccardi, "Pyramid Wavefront Sensor Behavior in Partial Correction Adaptive Optics Systems," Astron. Astrophys. **369,** L9–L12 (2001).
12. I. Iglesias, R. Ragazzoni, Y. Julien, and P. Artal, "Extended Source Pyramid Wave-Front Sensor for the Human Eye," Opt. Express **10,** 419–428 (2002), http://www.opticsexpress.org/abstract.cfm?URI=OPEX-10-9-419.
13. P. Artal, S. Marcos, R. Navarro, and D. R.Williams, "Odd Aberrations and Double-Pass Measurements of Retinal Image Quality," J. Opt. Soc. Am. A **12,** 195–201 (1995).
14. European Standard / EN60825-1:1993/A2:2001, European Committee for Electrotechnical Standardization (2001).
15. E. Dalimier and J. C. Dainty, "Comparative Analysis of Deformable Mirrors for Ocular Adaptive Optics," Opt. Express **13,** 4275–4285 (2005), http://www.opticsexpress.org/abstract.cfm?URI=OPEX-13-11-4275.
16. P. M. Prieto, E. J. Fernandez, S. Manzanera, and P. Artal, "Adaptive Optics With a Programmable Phase Modulator: Applications in the Human Eye," Opt. Express **12,** 4059–4071 (2004), http://www.opticsexpress.org/abstract.cfm?URI=OPEX-12-17-4059.
17. H. Hofer, L. Chen, G. Y. Yoon, B. Singer, Y. Yamauchi, and D. R. Williams, "Improvement in Retinal Image Quality With Dynamic Correction of the Eyes Aberration," Opt. Express **8,** 631–643 (2001), http://www.opticsexpress.org/abstract.cfm?URI=OPEX-8-11-631.
18. L. N. Thibos, A. Bradley, and X. Hong, "A Statistical Model of the Aberration Structure of Normal, Well-Corrected Eyes," Ophthal. Physl. Opt. **22,** 427–433 (2002).
19. W. S. Stiles and B. H. Crawford, "The Luminous Efficiency of Rays Entering the Eye Pupil at Different Points," Proc. R. Soc. Lond. B. **112,** 428–450 (1933).
20. L. Diaz-Santana, C. Torti, I. Munro, P. Gasson, and J. C. Dainty, "Benefits of Higher Closed-Loop Bandwidths in Ocular Adaptive Optics," Opt. Express **11,** 2597–2605 (2003), http://www.opticsexpress.org/abstract.cfm?URI=OPEX-11-20-2597.
21. T. Nirmaier, C. A. Diez, and J. F. Bille, "High Speed CMOS Wavefront Sensor With Resisting Ring Networks of Winner-Take-All Circuits," IEEE Journal of Solid-State Circuits **40,** 2315–2322 (2005).

1. Introduction

Since a first implementation in 1997 [1], adaptive optics (AO) systems for ophthalmic applications [2, 3, 4, 5, 6] have always relied on Shack-Hartmann sensors (SHS) [7] to perform wavefront sensing. While this choice was obviously successful in most cases, one could also think of alternative wavefront sensing approaches to achieve this task with possibly higher efficiency and greater flexibility.

The pyramid wavefront sensor (PS) was originally proposed [8] and implemented [9] within the astronomical community. Similar to a Foucault knife edge test, the aberration induced inhomogeneities are sensed by placing in the focal plane a four-facet pyramid refractive element with its tip aligned to the optical axis. The wavefront gradients along two orthogonal directions are retrieved from the intensity distribution among the four pupils images resulting from this operation. Under specific configurations, the PS offers a greater flexibility than the SHS as both pupil sampling and sensing sensitivity can be adjusted separately. Furthermore, numeric simulations comparing the SHS and PS suggest that the latter may operate with a higher sensitivity in closed-loop for astronomical applications [10, 11].

The application of the PS to ocular wavefront measurements was the object of a first study by Iglesias et al. who concluded to the feasibility of the technique [12]. This work outlined the flexibility of the PS for measuring a broad range of ocular aberrations but also pointed out the necessity to deal with the negative influence of spurious reflections from the anterior ocular surfaces. Considering the absence of an adequate statistical description of ocular aberration allowing performance simulation for an AO system using a PS, we built such an optical setup and studied its performance for ophthalmic applications.

#9724 - $15.00 USD Received 28 November 2005; revised 2 January 2006; accepted 5 January 2006

2. Apparatus

The instrument was designed for sensing and compensating ocular aberrations over a 6 mm diameter pupil at 635 nm (Fig. 1). The ocular aberration was measured in a non-symmetric double-pass manner with a probing collimated light beam of diameter 1.5 mm entering the eye at 2 mm off-axis. This optical configuration was required for ocular aberration measurements to avoid any difficulties associated with a symmetric double-pass measurement [13]. Furthermore, the beam diameter and off-axis entrance point into the eye of the probing laser beam were selected with a ray tracing software to avoid light reflected at each of the ocular surface to reach the wavefront sensor CCD. The power of the laser probing beam was 5 μW, thus preventing ocular light hazards for continuous eye exposures up to 30 minutes [14]. An optical trombone of variable length consisting of four mirrors with two of them mounted on a manual translation stage was used for compensating the subject's natural defocus, while the higher order aberration terms were compensated using a piezoelectric deformable mirror (diameter 30 mm, 19-actuators, 8-bit PCI controller; Flexible Optical B.V., Delft, The Netherlands) conjugated to the ocular pupil. Comparative simulations of the effectiveness of this mirror for ophthalmic use can be found in [15]. This deformable mirror was itself optically conjugated to a steering mirror (FSM-300, Newport, Irvine, CA, USA) positioned in the wavefront sensing arm, whose movement was controlled with two sinusoidal signal (100 Hz) of same amplitude A_0 and $\pi/2$ phase difference. This element produced a circular rotation of the point spread function around the tip of a custom made diffractive pyramid element (178 ° vertex angle, 7 mm diameter free aperture) positioned in the following focal plane. A scientific CCD camera (Retiga EX, QImaging, Burnaby, BC, Canada) recorded the 4 pupils imaged behind the pyramid element produced during a full rotation cycle. A calibration arm delivered a collimated reference beam to the wavefront sensing arm for closed-loop operation.

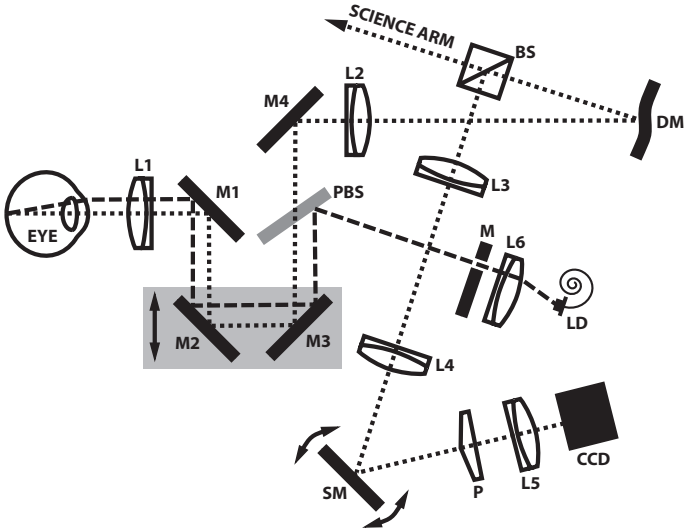

Fig. 1. Schematic optical setup showing the trajectory of the ingoing probing laser beam (dashed line) and the outgoing backscattered light (dotted line). L1-L6 achromat doublet lenses, M1-M4: mirrors, BS: beam splitter, PBS: pellicle beam splitter, M: mask, LD: laser diode (635 nm), DM: deformable mirror, SM: steering mirror, P: refractive pyramid element, CCD: charged coupled device

The ocular pupil was illuminated by means of infrared LEDs (880 nm) placed circularly in

#9724 - $15.00 USD Received 28 November 2005; revised 2 January 2006; accepted 5 January 2006

front of the eye and imaged on a low grade CCD camera, which allowed monitoring the pupil position during measurements.

A custom graphic user interface written under Labview (National Instruments, Austin, TX, USA) allowed full camera and mirror control. For each CCD readout frame (Fig. 2), the software registers the position of each of the 4 pupil intensity images and computes two maps proportional to the vertical and horizontal wavefront gradient based on formulas derived from a geometrical approximation:

$$\left.\frac{\partial\theta(x,y)}{\partial x}\right|_{(i,j)} \cong \frac{R}{F}\Delta\widehat{I}_x|_{(i,j)} = \frac{R}{F}\left.\left(\frac{I_2+I_4-I_1-I_3}{I_1+I_2+I_3+I_4}\right)\right|_{(i,j)} \quad (1)$$

$$\left.\frac{\partial\theta(x,y)}{\partial y}\right|_{(i,j)} \cong \frac{R}{F}\Delta\widehat{I}_y|_{(i,j)} = \frac{R}{F}\left.\left(\frac{I_1+I_2-I_3-I_4}{I_1+I_2+I_3+I_4}\right)\right|_{(i,j)} \quad (2)$$

where the horizontal and vertical gradients of the bi-dimensional phase function $\theta(x,y)$ evaluated at each pixel (i,j) are proportional to the normalized intensity difference along x and y, respectively $\Delta\widehat{I}_x$ and $\Delta\widehat{I}_y$, with I_1, I_2, I_3 and I_4 standing for the intensity in the upper-left, upper-right, lower-left and lower-right pupil, respectively. The scaling factor R/F quantifies the modulation tilt angle where R is the radius of the circular trajectory followed by the focal spot on the pyramid and F the distance between the steering mirror and the pyramid. This angle can also be expressed as a multiple of the unitary tilt angle λ/D where D is the diameter of the pupil image on the steering mirror.

The mirror commands required for compensating ocular aberrations are calculated directly from the two resulting gradient maps through a zonal control approach. Wavefront maps were retrieved by post-processing the recorded gradient maps using a least squares algorithm.

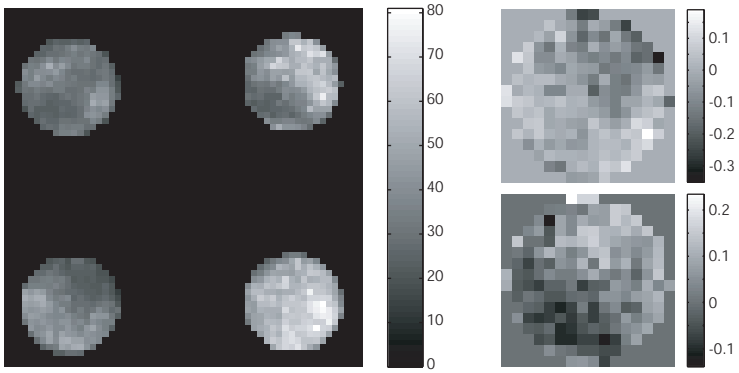

Fig. 2. Left: Typical *in vivo* CCD frame (65×65 pixels) obtained for a 10 ms integration time at 4×4 binning with an angular tilt modulation of $21\lambda/D$. Right: horizontal and vertical gradient maps calculated from this intensity image

The system was calibrated for closed-loop operation with no CCD binning and 4x4 binning and modulation tilt values of 7, 14, 21 and 28 λ/D. For each of these settings combination, the system acquired two gradient maps for each actuator (k) when set at both maximum ($\Delta\widehat{I}(k,Cmax)_x$, $\Delta\widehat{I}(k,Cmax)_y$) and minimum ($\Delta\widehat{I}(k,Cmin)_x$, $\Delta\widehat{I}(k,Cmin)_y$) of the command range while all other actuators sat at their bias position. From these data, two maps representing the gradient change over the full command range were then calculated ($\Delta\widehat{I}(k,Crange)_x$, $\Delta\widehat{I}(k,Crange)_y$), reshaped and combined into a column vector of a $19\times(2\cdot N)$ matrix, where N is the number of pixels of interest contained within the pupil. The pseudo-inverse of this

#9724 - $15.00 USD Received 28 November 2005; revised 2 January 2006; accepted 5 January 2006

matrix was then calculated using singular value decomposition and used as the control matrix for closed loop command of the adaptive mirror.

3. Open-loop bench test of sensing accuracy

An artificial "emmetropic" eye consisting of a positive doublet lens (f = 100 mm) with a black screen placed at its focal plane was mounted on the setup.

Small localized deformations of the mirror were obtained by applying to the central actuator command values C between -10 and +10 discrete levels of the 8-bit controller around the bias position. Sets of gradient maps $\Delta\widehat{I}(1,C)_x$ and $\Delta\widehat{I}(1,C)_y$ where recorded for each deformation. Fig. 3 shows the root mean square (RMS) value for each of the optical path difference (OPD) maps reconstructed from this measurement set. The results obtained for two modulation amplitudes illustrate the measurement accuracy that the PS can achieve. Thus, the highest modulation allows a linear measurement of small actuator displacements corresponding to single discrete levels of the 8-bit command range, while accuracy clearly degrades when using higher modulation value. If assuming a linear behavior of the piezoelectric actuator, it implies that our PS system can sense localized mirror deformation as small as approximately 25 nm corresponding to an OPD of $\lambda/13$. The average light intensity within the recorded pupil images amounted approximately 80/255 analog-to-digital units (ADU) with a 10 ms integration time, which indicates that our CCD operated in a photon noise limited regime considering its specifications (6 e^-/ADU, 8 e^- readout noise). Therefore, a modulation reduction inducing sectorial improvements of the signal to noise ratio within the pupil images collected by the CCD led to the global improvement of the PS precision that we observed in the present context.

The system was also operated in closed-loop at the 4 different modulation amplitudes while placing in front of the artificial eye different ophthalmic trial lenses ranging -1 to +1 diopter by step of 0.25 diopter. Consistent with the results presented above, the best aberration correction was obtained at the smallest modulation amplitude for all tested lenses with an average RMS residual improvement of 0.026 μm between corrections operated at 7 λ/D and 28 λ/D. When the system was operated in closed-loop without placing any lens in front of the artificial eye, the system measured residual RMS aberration of 0.016 μm at 7 λ/D and 0.048 μm at 28 λ/D, which indicates the ultimate correction level that this AO system can achieve.

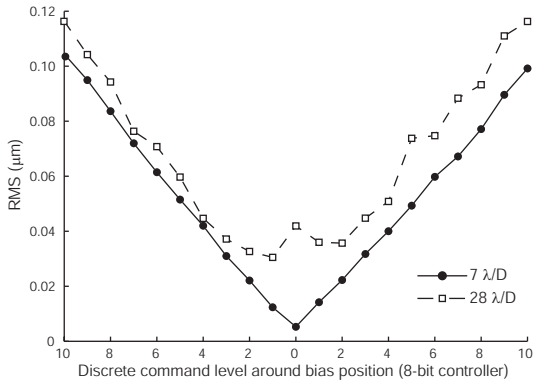

Fig. 3. RMS values of the reconstructed OPD map for a range of commands applied to the central actuator, while all other actuator are set at the bias position. The upper and lower curves correspond to RMS values obtained when sensing the wavefront with modulations of 28 and 7 λ/D, respectively, showing a clear reduction in RMS error for the lower modulation case

#9724 - $15.00 USD Received 28 November 2005; revised 2 January 2006; accepted 5 January 2006

4. *In vivo* operation

Ocular aberrations were compensated in closed-loop with the instrument on 4 dilated eyes. A bite bar mounted on micrometric linear stages provided the necessary head stability and allowed precise positioning of the ocular pupil relatively to the instrument. The pupil position was monitored in the infrared (880 nm) between each measurement session by means of a dichroic filter placed at 45 ° in between the eye and L1 (Fig. 1) and reflecting light into a pupil imaging arm. The subject was instructed to use the probing beam as a fixation target during the measurements. As a preliminary step, the subject was also asked to maximize the apparent spot sharpness by manually adjusting the length of the optical trombone, thus compensating for the focus error of the eye.

With a 5 μW probing power, the integration time required for recording in a 4×4 binning mode a CCD frame of 65×65 pixels containing the 4 pupil images was 10 ms (Fig. 2). Each pupil was thus sampled through a grid of 16×16 pixels and the system achieved stable closed-loop correction at a rate of 55 Hz with a correction gain value of 0.5 (Fig. 4). The bulk of aberration correction occurred within the first second of closed-loop operation.

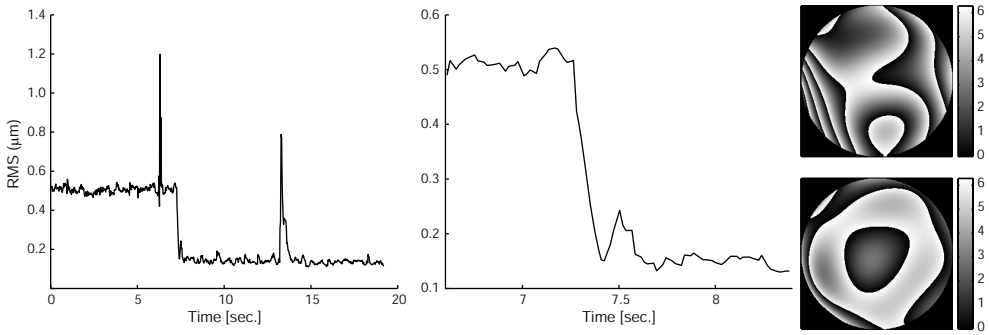

Fig. 4. Left: Time evolution of the optical path difference RMS as recorded on a volunteer while closing the adaptive loop (7 λ/D modulation). Each spike corresponds to an eye blink. Center: Enlarged sequence showing the onset of the closed-loop correction. Right: maps of the wrapped phase before (up) and during (down) closed-loop operation

Closed-loop corrections were successfully obtained on 4 different eyes with 4 different modulation amplitudes and we observed that the average residual RMS of the wavefront error with a tilt modulation of 7 λ/D was substantially lower (59%) than with a 4 times larger modulation (Fig. 5). Furthermore, the simultaneous recording of the commands sent to the actuators of the deformable mirror indicate that the average variance on the 19 channels similarly decreases by 73% (Fig. 5).

The residual RMS values of the wavefront error achieved with our system (0.14 – 0.34 μm RMS residual) for angular tilt modulation between 7 and 28 λ/D are in the range of the values obtained with other AO systems [4, 15, 16, 17] and it appears that lower modulation amplitudes improves the ability of the system to compensate for ocular aberrations as the residual RMS drops to 0.14 ± 0.004 μm for 7 λ/D. This improvement quite closely correlates to a decrease of the variance of the command corrections sent to the deformable mirror which shows how the PS, in closed-loop operation, can improve AO performance by sensing ocular aberrations with greater accuracy. At this stage, it appears difficult to compare the absolute performance of the PS and SHS sensors when operated in closed-loop as other existing ophthalmic AO systems use different corrective optical elements or perform aberration correction on different pupil sizes. The performance of an AO system depends on the efficiency of the wavefront sensor but also

#9724 - $15.00 USD Received 28 November 2005; revised 2 January 2006; accepted 5 January 2006

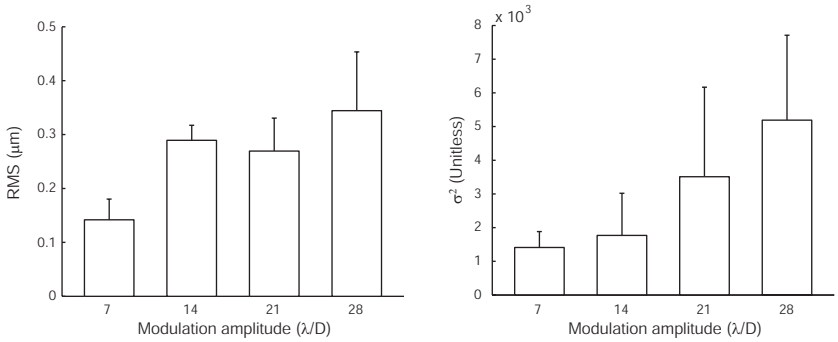

Fig. 5. Left: Residual optical path difference RMS achieved during closed-loop correction for different modulation amplitude. Right: Average variance on the command corrections sent to the mirror for the same range of modulation amplitudes

on the ability of the deformable mirror to shape ocular aberrations. A simulation using the measured influence function of each actuator along with a statistical model of ocular aberration [18] showed that our 19-actuator mirror can achieve a residual RMS of 0.17 μm over a 6 mm pupil [15], a correction level consistent with the 0.14 μm RMS residual (7 λ/D modulation) obtained with our system. In order to check the effect of the AO correction, a CCD aligned in a conjugated retinal plane of the scientific arm (Fig. 1) was used to record the double-pass ocular point spread function (PSF). We observed in every measured eye a marked reduction of the PSF spatial extend and a significant increase of its contrast when operating the system in closed-loop (Fig. 6).

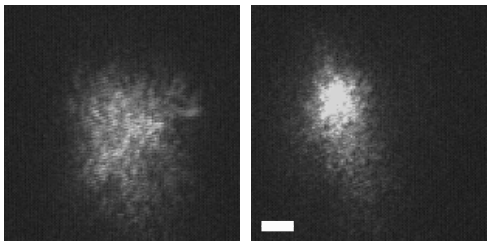

Fig. 6. Left: Double-pass ocular PSF recorded in one eye in open- (left) and closed-loop (right) conditions (21 λ/D modulation). In diffraction limited conditions, the probing beam has an Airy diameter of 13 μm at the retina and 42 μm on the imaging CCD. White scale bar: 100 μm

While, this study was conducted with a predefined arbitrary set of modulation amplitudes, the results suggest that the system could eventually achieve higher corrections by reducing the modulation radius. One could argue that further increasing wavefront sensing sensitivity would come at the expense of a reduction of the sensing linear range. Thus, reducing the modulation amplitude increases the amplitude of intensity variations among the 4 pupil images and some CCD pixels eventually become saturated, which limits the sensor ability to correctly retrieve ocular aberrations in open loop. However, this problem does not seem to affect closed-loop operation as long as the system succeeds in calculating a set of correctly signed command corrections, which was the case with the lower modulation settings used in the present work. Should this issue become a problem, then one could think of using different modulation amplitudes and switching between them while closing the loop depending of the aberration range to

#9724 - $15.00 USD Received 28 November 2005; revised 2 January 2006; accepted 5 January 2006

correct, thus effectively evolving toward an optimized dynamic correction.

The intensity profile across the ocular pupil resulting from light backscattering at the retina shows a variation, an effect named after Stiles & Crawford who attributed it to the directionality of light transport along photoreceptors [19]. Because light detection for pyramid sensing is performed in a conjugated pupil plane, it appears quite straightforward to estimate this effect in open-loop by using the intensity sum $(I_1+I_2+I_3+I_4)|_{(i,j)}$ computed at the denominator of Eq. (1) and (2). This information could be included in the post-hoc analysis of the open-loop data or eventually as an input for control optimization in closed-loop.

The PS retrieves wavefront gradient information by measuring intensity differences between regions of CCD readout frames. As each pixel (i,j) of the gradient information maps $\Delta\widehat{I}_x$ and $\Delta\widehat{I}_y$ described in Eq. (1) and (2) is normalized by the total intensity collected among the 4 pupils for this specific pixel, pyramid wavefront sensing is theoretically insensitive to smooth intensity variations within the system entrance pupil. However, the validity of this argument should be questioned as soon as pixels values within the 4 measured pupils enter a noise dominated regime or in the case of sharp intensity changes. Unlike astronomy where the intensity distribution is fairly constant across the entrance pupil of the telescope and scintillation is small for reasonably good observation conditions, double-pass measurements of ocular aberration present non-negligible intensity variations within the ocular pupil. Thus, while the Stiles-Crawford effect previously mentioned induces pupil apodization, one can also expect to observe in the pupil localized and highly contrasted intensity variations, known as speckle, due the coherence of the probing laser source. Such features appear in intensity frames recorded *in vivo* without binning the CCD pixels, which produced $\sim$ 3200 pixels of interest within the pupil, however the contrast of these speckles clearly decreases when reducing the pupil sampling and CCD frames recorded with our adaptive optics settings at 4×4 binning show rather smooth intensity variations (Fig. 2). This indicates that a coarse pupil sampling as used for closed-loop operation with the PS greatly reduces the speckle effect. In an attempt to evaluate the influence of speckle on wavefront gradient maps obtained with the PS, we compared individual gradient maps calculated from a single CCD frame (10 ms) to average gradient maps based on 300 CCD frames collected over 5 seconds on the same eye (Fig. 7). As constant movements of the eye modify scattering at the retinal tissue level, our hypothesis was that while individual gradient maps could show abrupt slope changes due to the presence of speckles in the intensity map, averaging several gradient maps collected at different times would result in a gradient information free of any speckle influence. Our measurements however showed that individual gradient maps, despite being noisier, essentially carried the same slope information. This result suggests that the PS, under some configurations, might be speckle noise resistant. An intuitive explanation that deserves further investigations would be that the speckle affecting the quality of the PSF in the focal plane also circulated around the tip of the pyramid and contribute to form 4

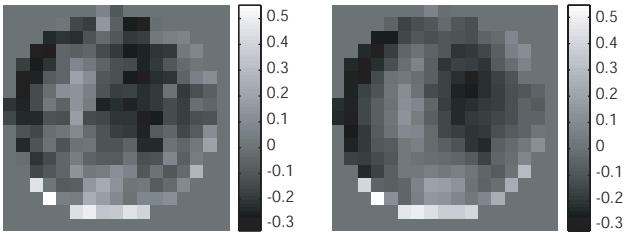

Fig. 7. Left: Individual $\Delta\widehat{I}_x$ map calculated from a single CCD intensity frame. Right: $\Delta\widehat{I}_x$ map resulting from the average of 300 individual $\Delta\widehat{I}_x$ collected within 5 sec. on the same eye

#9724 - $15.00 USD Received 28 November 2005; revised 2 January 2006; accepted 5 January 2006

pupil intensity images where speckle is spatially correlated. Thus, speckle information cancels out to first order when retrieving the gradient maps by computing $\Delta\widehat{I_x}$ and $\Delta\widehat{I_y}$. As the quality of the focal spots in a SHS also degrades when speckle is present, thus affecting wavefront sensing accuracy, solutions such as broadband probing source, beam scanning or rotating diffusers have been used quite successfully in existing AO systems to solve this problem. While these solutions could allow recording speckle-free intensity images with the PS, they do not appear to be mandatory to retrieve aberration information.

Our wavefront sensor uses the beam circulation strategy originally proposed for PS by Ragazzoni [8], which allows a control of the aberration measurements sensitivity. An alternative approach using an extended source was also devised and tested for ophthalmic application [12]. While both are theoretically justified and should provide the same results, we believe that beam circulation offers more flexibility for AO applications as the sensing sensitivity can be controlled dynamically through the amplitude of the steering modulation.

With roughly 200 pixels of interest when operating the CCD in 4×4 binning mode, the pupil sampling was unnecessarily high for operating a 19 actuator mirror in closed-loop and a similar level of performance could probably be achieved if reducing the sampling by a factor of 2. The integration time needed to record such CCD frames with the same probing power would thus decrease to approximately 2 – 3 ms and one could reasonably think, with additional minor system improvements, of achieving very fast ocular wavefront measurement at a rate of $\sim$ 1 kHz, which would be a significant improvement compared to the fastest ophthalmic SHS ever reported [20, 21]. In the light of the previous argument, the PS does not appear limited in the dynamical rate behavior and we believe that it could become a wavefront sensor of choice for fast ophthalmic AO systems.

5. Conclusion

Pyramid wavefront sensing can be used for ophthalmic adaptive optics and the present work suggests that it might help improving the aberration compensation efficiency by sensing aberrations with a greater accuracy or allowing higher closed-loop bandwidth than with Shack-Hartmann wavefront sensors. While these results remain to be validated by obtaining diffraction limited images of the retina and carrying a strict analysis of their spatial frequency content, we believe that the levels of residual aberration correction measured during closed-loop operation strongly encourage the use of the pyramid sensor. Interestingly, pyramid sensing appeared rather insensitive to the presence of speckle and this issue will deserve further investigations, as aberration measurements in the ophthalmic context but also in other fields, often suffer from the presence of speckle.

Acknowledgement

This work was supported by Science Foundation of Ireland under Grant 01/PI.2/B039C.

#9724 - $15.00 USD Received 28 November 2005; revised 2 January 2006; accepted 5 January 2006